Energy & Environmental Science

www.rsc.org/ees

Volume 3 | Number 8 | August 2010 | Pages 981–1136

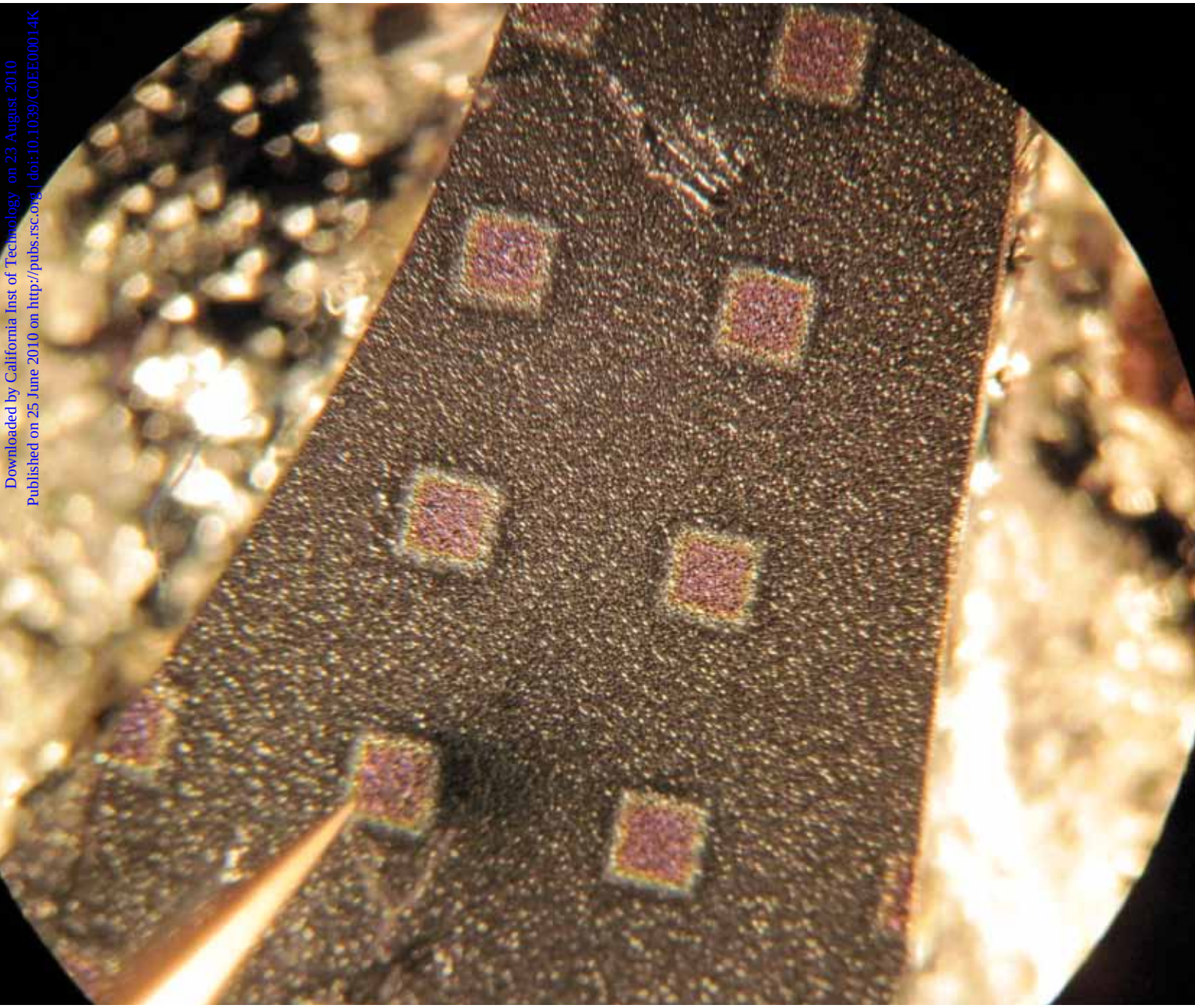

ISSN 1754-5692

RSC Publishing

COVER ARTICLE
Atwater and Lewis *et al.*
Si microwire-array solar cells

PERSPECTIVE
Park and Holt
Recent advances in nanoelectrode achitecture for photochemical hydrogen production

Si microwire-array solar cells†

Morgan C. Putnam,[ab] Shannon W. Boettcher,[a] Michael D. Kelzenberg,[b] Daniel B. Turner-Evans,[b] Joshua M. Spurgeon,[a] Emily L. Warren,[a] Ryan M. Briggs,[b] Nathan S. Lewis*[ac] and Harry A. Atwater*[bc]

Received 5th April 2010, Accepted 18th May 2010
DOI: 10.1039/c0ee00014k

Si microwire-array solar cells with Air Mass 1.5 Global conversion efficiencies of up to 7.9% have been fabricated using an active volume of Si equivalent to a 4 μm thick Si wafer. These solar cells exhibited open-circuit voltages of 500 mV, short-circuit current densities (J_{sc}) of up to 24 mA cm^{-2}, and fill factors >65% and employed Al_2O_3 dielectric particles that scattered light incident in the space between the wires, a Ag back reflector that prevented the escape of incident illumination from the back surface of the solar cell, and an a-SiN_x:H passivation/anti-reflection layer. Wire-array solar cells without some or all of these design features were also fabricated to demonstrate the importance of the light-trapping elements in achieving a high J_{sc}. Scanning photocurrent microscopy images of the microwire-array solar cells revealed that the higher J_{sc} of the most advanced cell design resulted from an increased absorption of light incident in the space between the wires. Spectral response measurements further revealed that solar cells with light-trapping elements exhibited improved red and infrared response, as compared to solar cells without light-trapping elements.

Vertically aligned arrays of crystalline-Si (c-Si) microwires may enable the fabrication of flexible c-Si solar cells with near unity internal quantum yield that are capable of absorbing >85% of the day-integrated (above band gap) direct solar illumination using a volume of Si equivalent to a 2.8 μm thick Si film.[1] Two advantages conferred by the three-dimensional geometry of vertically aligned, high-aspect ratio Si microwires are: (1) the ability to create high-quality single crystal Si structures with passivated surfaces *via* a vapor growth process;[2–4] and (2) enhanced absorption relative to planar c-Si absorbers.[1] These two advantages, in combination with the ability to grow arrays of Si microwires over large areas (>1 cm^2),[5] to peel the wire arrays from the growth substrate in a flexible polymer,[6] and to re-use the growth substrate,[7] offer the potential to fabricate flexible, high efficiency c-Si solar cells.[8,9]

Wire solar cells have been fabricated using c-Si,[10–20] amorphous-Si,[21] GaAs,[22] III-nitride,[23] and InP,[24] *via* a variety of growth techniques, including vapor-liquid-solid (VLS) growth,[10–16,19,20] metal-catalyzed chemical etching,[17,21] molecular beam epitaxy,[22] metal–organic chemical vapor deposition,[23,24] and deep reactive-ion-etching.[18] In particular, the VLS growth method offers a materials-efficient and scalable route for the synthesis of semiconducting wires. However, the efficiencies of VLS-grown, c-Si, single-wire[13,14,16] and wire-array[10–12,15,19,20] solar cells, up to 3.4%[13] and 1.8%[15] respectively, have fallen short of the ~15% photovoltaic efficiency predicted from simple considerations.[8,9] In particular these solar cells have failed to demonstrate open-circuit voltages (V_{oc}) in excess of 300 mV, possibly indicative of significant recombination within the depletion region and/or at the surfaces of the cells.[8,12,25] We report c-Si microwire-array solar cells that have exhibited 7.9% conversion of simulated Air Mass (AM) 1.5 Global (G) solar illumination to electrical energy with negligible photovoltaic response from the growth substrate.

Square-tiled arrays of vertically aligned Si microwires (2–3 μm in diameter on a 7 μm pitch) were grown on p^{++} (resistivity, ρ, <0.001 Ω cm) Si(111) wafers using the VLS growth method, as described previously.[5] P-type doping of the Si microwires was achieved during growth using BCl_3 as a gaseous dopant source.[4] Four-point electrical measurements performed on individual Si wires from arrays grown

[a]*Division of Chemistry and Chemical Engineering, California Institute of Technology, 1200 E. California Blvd, Pasadena, CA, 91125, USA. E-mail: nslewis@caltech.edu; Fax: +1 626 395-8867; Tel: +1 626 395-6335*
[b]*Thomas J. Watson Laboratories of Applied Physics, California Institute of Technology, 1200 E. California Blvd, Pasadena, CA, 91125, USA. E-mail: haa@caltech.edu; Fax: +1 626 844-9320; Tel: +1 626 395-2197*
[c]*Kavli Nanoscience Institute, California Institute of Technology, 1200 E. California Blvd, Pasadena, CA, 91125, USA*

† Electronic supplementary information (ESI) available: Experimental methods and additional solar cell characterization are presented. See DOI: 10.1039/c0ee00014k

Broader context

Driven by the restructuring of Germany's Renewable Energy Sources Act in 2000, the photovoltaics industry has grown tremendously, demonstrating an average compound annual growth rate of 56% in the five-year period prior to 2008. As a result of this growth and the subsequent development of the industry, the cost of photovoltaic electricity will likely reach grid-parity within the next 6–10 years (without significant technological advances.) However, for photovoltaics to generate an appreciable fraction of electricity, costs must be further reduced such that energy storage systems (batteries, hydrogen production coupled with fuel cells) can be implemented. Recently, Si microwire-array solar cells have emerged as a promising new type of low-cost solar cell with the potential for dramatically reduced Si consumption and flexible modules, while offering c-Si photovoltaic efficiencies. In this work we demonstrate the fabrication of Si microwire-array solar cells with high open-circuit voltages, short-circuit current densities and fill factors. These solar cells exhibit photovoltaic efficiencies of up to 7.9% and should achieve efficiencies of ~15% with known improvements in cell design.

under nominally identical conditions indicated that the wires were p-type with $\rho = 0.05\ \Omega$ cm, which corresponds to an electrically active dopant concentration (N_A) of 7×10^{17} cm^{-3}, assuming a bulk hole mobility of 1.8×10^2 cm^2 V^{-1} s^{-1} for Si.

Radial p–n junctions were fabricated within each wire, as illustrated in Fig. 1. First, the as-grown wire arrays (Fig. 1a) were chemically etched to remove the Cu-catalyst and to remove a thin layer (~50 nm) of surface Si, prior to the growth of a 200 nm thick thermal oxide (Fig. 1b). The thermal oxide was then selectively removed in a hydrofluoric acid (HF) solution (aq.), using polydimethylsiloxane (PDMS) as an etch barrier for the thermal oxide located at the bases of the microwires (Fig. 1c). After removal of the PDMS,[26] radial p–n junctions were formed in the upper region of the Si microwires during a phosphorus diffusion (junction depth of ~80 nm in a planar control), while the thermal oxide functioned as a phosphorus diffusion barrier for the lower region of the wires (Fig. 1d). We note that by appropriate choice of the PDMS layer thickness, the p–n junction could be defined to approximate either a radial or an axial p–n junction, or some combination of the two.

Three different types of Si microwire solar cells were fabricated. The As-Grown cell contained no light trapping elements or surface passivation. The Scatterer cell incorporated light-scattering Al_2O_3 particles (nominally 80 nm in diameter) in-between the wires. The *PRS* cell utilized an a-SiN$_x$:H passivation layer to minimize surface recombination and to serve as an anti-reflection coating, a Ag back reflector to prevent the loss of incident illumination into the growth substrate, and Al_2O_3 particles to scatter light incident between the Si microwires. Following the inclusion of the selected light-trapping elements (see ESI†), each wire array was filled to the tips of the wires with mounting wax (a transparent, non-conducting, thermoplastic polymer). Indium tin oxide (ITO) (120–150 nm thick, $\rho \approx 7 \times 10^{-4}\ \Omega$ cm) was then sputtered through a shadow mask to form a top-contact pad and to define individual cells.

Fig. 2 displays cross-sectional scanning electron microscope (SEM) images of a wire array after p–n junction formation and of a microwire solar cell for each cell type. As seen in Fig. 2a, the height of the thermal oxide (and thus the extent of the radial p–n junction) was uniform across the wire array. Wire heights ranged from 57–63 μm, 71–78 μm, and 43–49 μm for the As-Grown (Fig. 2b), Scatterer (Fig. 2c), and PRS (Fig. 2d) microwire solar cells, respectively. The thermal oxide covered the lower 27–32 μm of the wires in the As-Grown and Scatterer solar cells, but was removed prior to the desorption of the a-SiN$_x$:H layer in the PRS solar cells. For both the Scatterer and PRS solar cells, the 80 nm Al_2O_3 particles were observed to form micron-sized agglomerates that were located near the base of the wires, as evidenced by the granular texture of the mounting wax near the bottom of the wire array (Fig. 2c and d) and at the wire tips and sidewalls (Fig. 2c and d, inset). In the PRS solar cells, the 1000 nm thick Ag back reflector covered the growth substrate and the tapered base of the wires (Fig. 2d and S1†). The a-SiN$_x$:H anti-reflection/passivation layer in the PRS cell is not visible in Fig. 2d. However, the a-SiN$_x$:H layer conformally coated the wires and substrate prior to selective removal of the a-SiN$_x$:H from the tips of the wires, which allowed for the ITO to contact the n-Si emitter (Fig. S2†). For all devices, the mounting wax uniformly infilled the wire array, and the ITO conformally coated the mounting wax and the wire tips, thereby providing a continuous top contact despite the highly textured surface.

An important consideration for measurements of the photovoltaic performance of wire-array solar cells is the contribution from the growth substrate to the observed photocurrent. Though the fabrication of an appropriate control cell is not straightforward (even if the emitter doping compensated the substrate doping, the n$^+$ emitter and p^{++} substrate would form a tunnel junction) significant photocurrent from the substrate can be ruled out in our microwire-array solar cells. For the As-Grown and Scatterer solar cells, scanning photocurrent microscopy measurements indicated an effective minority-carrier diffusion length < 0.5 μm for electrons in the thermal-oxide-coated bases of the wires.[3] Consequently, neither the growth substrate nor the lower 27–32 μm of the wires contributed significantly to the observed photocurrent of the As-Grown and Scatterer solar cells. For the PRS microwire solar cells, the removal of the thermal oxide, followed by the deposition of the a-SiN$_x$:H passivation layer, produced an effective electron minority-carrier diffusion length ≫ 30 μm in the p-type bases of the wires.[3] Taken together, these results suggest that the bulk minority-carrier diffusion length is ≫ 30 μm throughout the wire but that the thermal-oxide-coated bases of the wires, for the Scatterer and As-Grown cells, exhibited very high surface recombination velocities, limiting the effective diffusion length in the oxide-coated wire bases to <0.5 μm. Hence, a photovoltaic response from the entire length of the wires was possible for the PRS solar cells. However, the photovoltaic contribution from the substrate for the PRS cells should be negligibly small, as the optically thick Ag back reflector coated the entire substrate except for where the wires had grown, ensuring that only the light guided through the Si microwires was able to reach the substrate. Consequently, 95% of the illumination ≤800 nm should have been absorbed over the 43–49 μm length of the wires, by a simple Beer–Lambert law analysis. The remaining illumination entered the p^{++} Si substrate (ρ < 0.001 Ω cm), which has been shown to exhibit an external quantum yield <0.05 for 800–1100 nm illumination.[1,2]

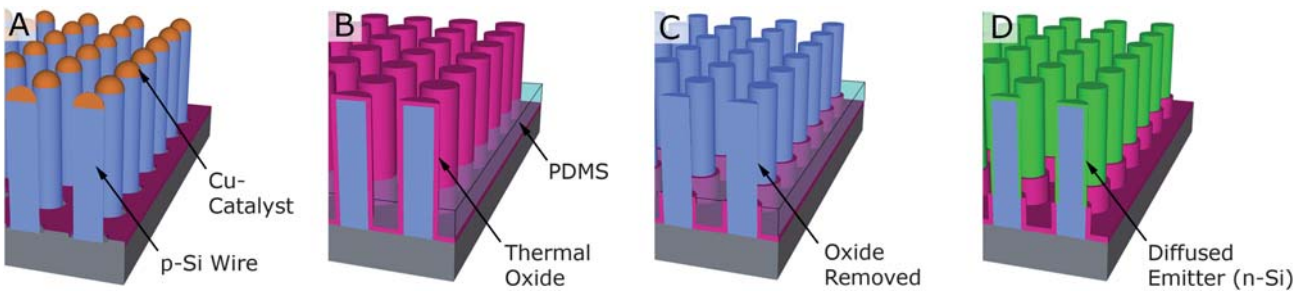

Fig. 1 Schematic of the radial p–n junction fabrication process. (a) VLS-grown, p-Si microwire array. (b) Microwire array after catalyst removal, growth of a thermal oxide and deposition of a PDMS layer. (c) Removal of the unprotected thermal oxide. (d) Removal of the PDMS and subsequent phosphorus diffusion to complete the fabrication of a radial p–n junction.

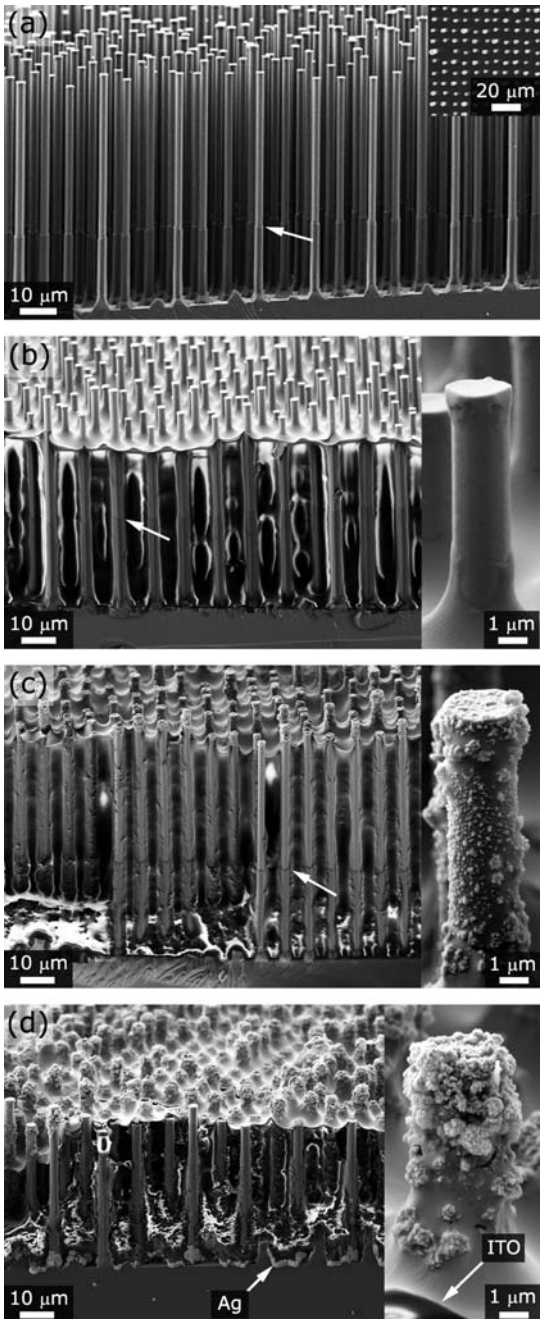

Fig. 2 Si microwire array solar cell device geometry. (a) Cross-sectional scanning electron microscope (SEM) image of a Si microwire array after radial p–n junction formation. The white arrow denotes the height of the thermal oxide (used as a phosphorus diffusion barrier in the radial p–n junction fabrication process). *Inset*: top-down SEM image of the same Si microwire array illustrating the pattern fidelity and slight variation in wire diameter. Cross-sectional SEM image of (b) an As-Grown solar cell, (c) a Scatterer solar cell, and (d) a PRS solar cell. *Insets*: higher magnification SEM images of the wire tips coated with ITO. For (b) and (c) the white arrow again denotes the height of the thermal oxide. For (d) the white arrow denotes the presence of the Ag back reflector. For the inset of (d) the white arrow denotes the ITO layer.

In total, 15 As-Grown microwire solar cells, 12 Scatterer microwire solar cells, and 24 PRS microwire solar cells were fabricated. The area of the fabricated cells spanned a range from 0.12 to 0.21 mm^2, as a result of variations in the gap between the top of the microwire arrays and the shadow mask during the deposition of the ITO. For each cell type, the majority of the cells were found to exhibit mutually similar V_{oc} and fill factor (FF) values (see Table S1†). To convert the measured short-circuit currents to short-circuit current densities (J_{sc}) and to calculate the photovoltaic efficiency (η), scanning photocurrent microscopy (SPCM) was used to image the perimeter of 2–3 cells from each cell type and thus accurately determine the photoactive cell area (see Fig. S3†).

Fig. 3 plots the measured current density as a function of voltage for the champion microwire solar cell of each cell type, in the dark (Fig. 3a) and under 100 mW cm^{-2} of simulated AM 1.5G illumination (Fig. 3b), respectively. In the dark, the microwire solar cells exhibited rectifying behavior with diode ideality factors between 1.7 and 2.2. The roll-off in the current density near 0.5 V in forward-bias resulted from the series resistance of the solar cells, which ranged from 300 to 3000 Ω and was dependent upon the quality of the contact between the electrical probe and the ITO.

Under simulated AM 1.5G illumination, the champion PRS solar cell exhibited markedly higher photovoltaic performance than the champion Scatterer and As-Grown solar cells, as a result of a significant increase in J_{sc} (Fig. 3b). Table 1 displays the values of V_{oc}, J_{sc}, FF, and η for all of the microwire solar cells whose cell areas were

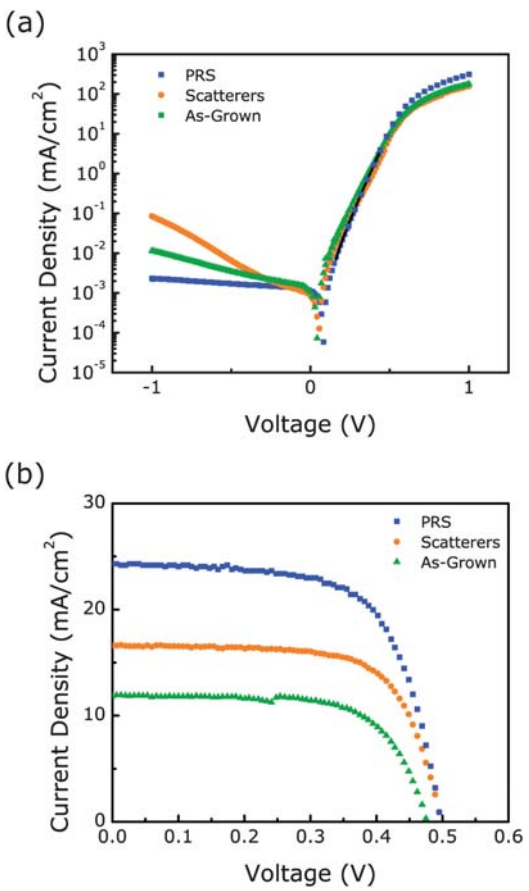

Fig. 3 Current density as a function of voltage for the champion microwire solar cell of each cell type (a) in the dark and (b) under simulated AM 1.5G illumination. The black line in (a) is an exponential fit to the dark *J*–*V* data of the PRS solar cell and was used to extract an ideality factor of 1.8.

measured by SPCM. V_{oc} of ~500 mV and FF > 65% were observed for all three cell types. The champion PRS solar cell produced a V_{oc} of 498 mV, J_{sc} of 24.3 mA cm^{-2}, and FF of 65.4%, for an $\eta = 7.92\%$. The champion Scatterer and As-Grown solar cells exhibited $\eta = 5.64\%$ and $\eta = 3.81\%$, respectively, with similar V_{oc} and FF but lower J_{sc}. For the PRS and Scatterer cells, the differences in η within a cell type largely resulted from differences in J_{sc}, which may have resulted from variations in the incorporation of the Al_2O_3 scattering particles or from variations in the fraction of electrically contacted wires (see Fig. 4b and c and S3†). We estimate the internal error in the measurement of the cell area to be 5% and the internal error in the AM 1.5G illumination intensity to be 5%, yielding a ~7% internal error in the measurement of J_{sc} and η.

To better understand the differences in J_{sc} between the PRS, Scatterer, and As-Grown solar cells, scanning photocurrent microscopy was used to map the photocurrent produced by the wire-array solar cells as a function of localized laser illumination ($\lambda = 650$ nm, ~1.0 μm beam waist), as seen in Fig. 4. To facilitate comparison between the different types of cells, each scanning photocurrent image was normalized to its maximum photocurrent. The measured photocurrent was maximized when the laser illumination was centered on a wire and was minimized when the illumination was centered between four adjacent wires. The photocurrent cross-sections shown below each scanning photocurrent image indicated that the relative magnitude of the decay in photocurrent as the laser moved from a peak (centered on a wire) to a valley (between two adjacent wires) clearly decreased from the As-Grown cell (Fig. 4a) to the Scatterer cell (Fig. 4b) and from the Scatterer cell to the PRS cell (Fig. 4c). In particular, the PRS solar cell exhibited nearly uniform photocurrent across the array, demonstrating that the Ag back reflector and Al_2O_3 dielectric scattering particles allowed for the effective collection of light incident between the wires.

Table 1 Photovoltaic performance under simulated AM 1.5G illumination. The champion solar cell from each cell type is bolded

Sample	V_{oc}/mV	J_{sc}/mA cm^{-2}	*FF* (%)	η (%)
As-Grown C2R3	482	11.2	69.4	3.75
As-Grown C4R6	**477**	**11.8**	**67.5**	**3.81**
Scatterer C2R4	**499**	**16.6**	**68.0**	**5.64**
Scatterer C3R3	504	15.2	68.8	5.28
PRS C2R5	503	22.2	66.1	7.38
PRS C3R5	500	22.8	67.2	7.65
PRS C4R5	**498**	**24.3**	**65.4**	**7.92**

The spots of greatly reduced photocurrent in the Scatterer and PRS solar cells arose from wires that were not electrically contacted by the ITO (wire vacancies would be expected to produce a photocurrent similar to the valley photocurrent, whereas, uncontacted wires parasitically absorb incident illumination). The small fraction of electrically inactive wires seen for the PRS and Scatterer cells likely results from the presence of Al_2O_3 scattering particles at the wire tips preventing the fabrication of a good electrical contact between the n^+-Si emitter and the ITO.

As seen in Fig. 5, the As-Grown and Scatterer solar cells exhibited similarly shaped spectral response curves (though different in absolute magnitude), both exhibiting a decline in the external quantum yield (EQY) at wavelengths >550 nm. By comparison, the PRS solar cell exhibited nearly constant EQY between 500 nm and 800 nm. The increased red and infrared response of the PRS cell presumably arose from light incident between the wires that was scattered multiple times from the Al_2O_3 scattering particles and the Ag back reflector. Integration of the observed EQY with the AM 1.5G solar spectrum predicted J_{sc} values of 13.3 mA cm^{-2}, 18.0 mA cm^{-2}, and 23.3 mA cm^{-2} for the As-Grown, Scatterer, and PRS solar cells, respectively, in good agreement with the measured J_{sc} values.

The three types of microwire solar cells were fabricated to facilitate a comparison between the cell types. However, three differences between the cells are worth noting. First, the wire length and thermal oxide heights translated to active wire lengths of 27–33 μm, 41–48 μm, and 43–49 μm for the As-Grown, Scatterer and PRS solar cells, respectively. Assuming no reflection losses and single-pass absorption, the theoretical increase in J_{sc} from a 30 μm thick Si wafer to a 45 μm thick Si wafer is 1.75 mA cm^{-2}, a 5.3% increase. Applying a 5.3% increase to the 11.8 mA cm^{-2} J_{sc} of the As-Grown champion

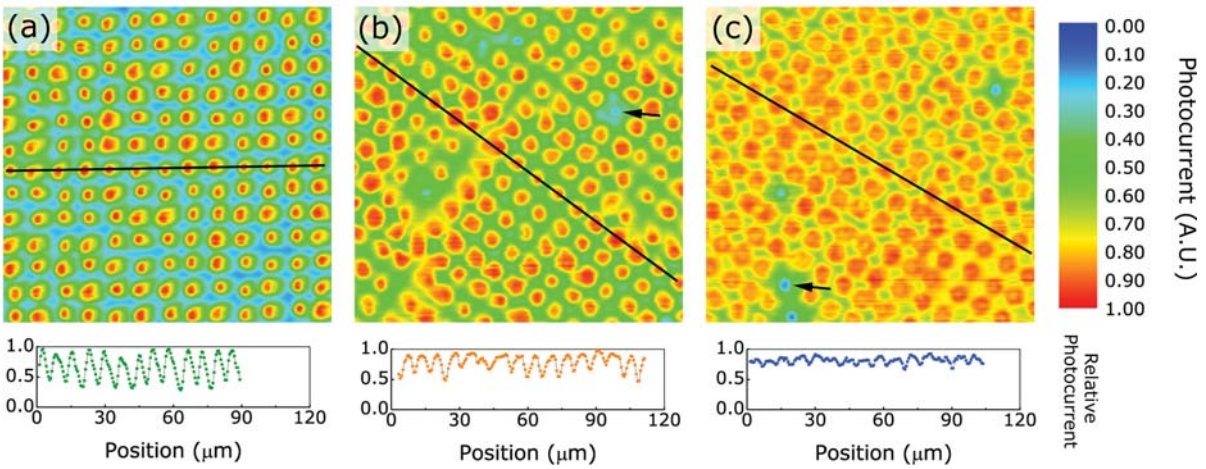

Fig. 4 Scanning photocurrent microscopy (SPCM) images and associated photocurrent line profiles from the center of (a) an As-Grown solar cell, (b) a Scatterer solar cell, and (c) a PRS solar cell. The SPCM images are 90 μm × 90 μm and were normalized to the maximum measured photocurrent in each image. The black lines on each SPCM image denote the cross-section used to produce the associated photocurrent line profiles. The black arrows denote spots of greatly reduced photocurrent believed to result from wires that were not in contact with the ITO.

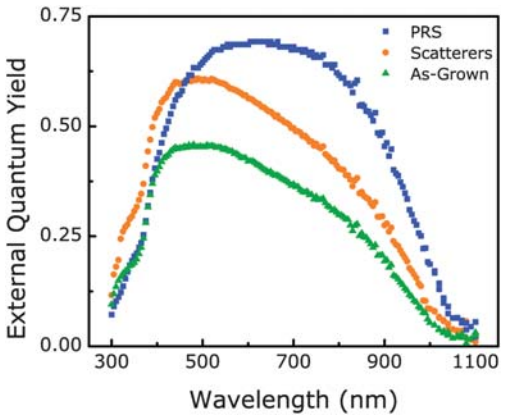

Fig. 5 Spectral response of the champion Si microwire solar cell of each cell type.

solar cell yields a J_{sc} of 12.4 mA cm^{-2}, well below the observed 16.6 mA cm^{-2} J_{sc} for the Scatterer champion solar cell. Thus, the additional active wire length alone cannot explain the increase in J_{sc} from the As-Grown solar cells to the Scatterer solar cells. Second, the Al_2O_3 scattering particles were largely located adjacent to the photo-inactive, thermal-oxide-coated, bases of the wires. Consequently, the full effect of the Al_2O_3 scattering particles is unlikely to have been seen in the Scatterer solar cells. Third, for the PRS and Scatterer cell types, ~2% of the wires in the center of the cell (Fig. 4) and 2–20% of the wires near the perimeter of the cell (Fig. S3†) were not electrically active. Thus, with improved contacting, the PRS and Scatterer cell types would be expected to produce a still slightly higher J_{sc} and η.

Recently, we have demonstrated single-wire solar cells with V_{oc} of up to 600 mV and FF of up to 82%.[3] Additionally, we have previously shown that wire-array photoelectrochemical cells can exhibit near-unity internal quantum yields.[1] Based on these measurements, efficiencies for wire arrays of ~15%, *as compared to the simple theoretical expectation of 17%*, could potentially be achieved by increasing the J_{sc} to 32 mA cm^{-2} (*e.g.*, by using longer wires and increasing the electrically active wire fraction, while accounting for parasitic absorption in the ITO and contact shading), by increasing the FF to 80% (through the addition of a metallic grid on the top contact), and by increasing the V_{oc} to 600 mV.[3] Separately, the design of our p–n junction, which does not extend to the base of the wire array, should prevent shunting of the p–n junction at the back contact in wire-array solar cells that have been removed from the growth wafer.

Acknowledgements

This work was supported by BP and in part by the Department of Energy (Basic Energy Sciences, Energy Frontier Research Center under grant DE-SC0001293 and also grant DE-FG02-07ER46405) and made use of facilities supported by the Caltech Center for Sustainable Energy Research, the Center for Science and Engineering of Materials—an NSF Materials Research Science and Engineering Center at Caltech (DMR 0520565), the Molecular Materials Research Center of the Beckman Institute at Caltech, and the Kavli Nanoscience Institute at Caltech. S.W.B. acknowledges the Kavli Nanoscience Institute for fellowship support, and D.B.T.-E. acknowledges the National Science Foundation for fellowship support. The authors acknowledge Dr Michael Walter for helpful discussions.

References

1 M. D. Kelzenberg, S. W. Boettcher, J. A. Petykiewicz, D. B. Turner-Evans, M. C. Putnam, E. L. Warren, J. M. Spurgeon, R. M. Briggs, N. S. Lewis and H. A. Atwater, *Nat. Mater.*, 2010, **9**, 239–244.
2 S. W. Boettcher, J. M. Spurgeon, M. C. Putnam, E. L. Warren, D. B. Turner-Evans, M. D. Kelzenberg, J. R. Maiolo, H. A. Atwater and N. S. Lewis, *Science*, 2010, 327, 185–187.
3 M. D. Kelzenberg, D. B. Turner-Evans, M. C. Putnam, S. W. Boettcher, R. M. Briggs, C. M. Baek, N. S. Lewis and H. A. Atwater, 2010, submitted.
4 M. C. Putnam, D. B. Turner-Evans, M. D. Kelzenberg, S. W. Boettcher, N. S. Lewis and H. A. Atwater, *Appl. Phys. Lett.*, 2009, **95**, 163116.
5 B. M. Kayes, M. A. Filler, M. C. Putnam, M. D. Kelzenberg, N. S. Lewis and H. A. Atwater, *Appl. Phys. Lett.*, 2007, **91**, 103110.
6 K. E. Plass, M. A. Filler, J. M. Spurgeon, B. M. Kayes, S. Maldonado, B. S. Brunschwig, H. A. Atwater and N. S. Lewis, *Adv. Mater.*, 2009, **21**, 325–328.
7 J. M. Spurgeon, K. E. Plass, B. M. Kayes, B. S. Brunschwig, H. A. Atwater and N. S. Lewis, *Appl. Phys. Lett.*, 2008, **93**, 032112.
8 B. M. Kayes, H. A. Atwater and N. S. Lewis, *J. Appl. Phys.*, 2005, **97**, 114302–114311.
9 M. D. Kelzenberg, M. C. Putnam, D. B. Turner-Evans, N. S. Lewis and H. A. Atwater, in 34th IEEE PVSC, Philadelphia, PA, 2009.
10 J. R. Maiolo, B. M. Kayes, M. A. Filler, M. C. Putnam, M. D. Kelzenberg, H. A. Atwater and N. S. Lewis, *J. Am. Chem. Soc.*, 2007, **129**, 12346–12347.
11 A. P. Goodey, S. M. Eichfeld, K. K. Lew, J. M. Redwing and T. E. Mallouk, *J. Am. Chem. Soc.*, 2007, **129**, 12344–12345.
12 L. Tsakalakos, J. Balch, J. Fronheiser, B. A. Korevaar, O. Sulima and J. Rand, *Appl. Phys. Lett.*, 2007, **91**, 233117.
13 B. Z. Tian, X. L. Zheng, T. J. Kempa, Y. Fang, N. F. Yu, G. H. Yu, J. L. Huang and C. M. Lieber, *Nature*, 2007, **449**, 885–889.
14 M. D. Kelzenberg, D. B. Turner-Evans, B. M. Kayes, M. A. Filler, M. C. Putnam, M. D. Kelzenberg, N. S. Lewis and H. A. Atwater, *Nano Lett.*, 2008, **8**, 710–714.
15 O. Gunawan and S. Guha, *Sol. Energy Mater. Sol. Cells*, 2009, **93**, 1388–1393.
16 T. J. Kempa, B. Z. Tian, D. R. Kim, J. S. Hu, X. L. Zheng and C. M. Lieber, *Nano Lett.*, 2008, **8**, 3456–3460.
17 K. Q. Peng, Y. Xu, Y. Wu, Y. J. Yan, S. T. Lee and J. Zhu, *Small*, 2005, **1**, 1062–1067.
18 E. C. Garnett and P. Yang, *Nano Lett.*, 2010, **10**, 1082–1087.
19 T. Stelzner, M. Pietsch, G. Andra, F. Falk, E. Ose and S. Christiansen, *Nanotechnology*, 2008, **19**, 295203.
20 B. M. Kayes, PhD , California Institute of Technology, 2009.
21 E. C. Garnett and P. D. Yang, *J. Am. Chem. Soc.*, 2008, **130**, 9224–9225.
22 C. Colombo, M. Heiss, M. Gratzel and A. F. I. Morral, *Appl. Phys. Lett.*, 2009, **94**, 173108.
23 Y. J. Dong, B. Z. Tian, T. J. Kempa and C. M. Lieber, *Nano Lett.*, 2009, **9**, 2183–2187.
24 H. Goto, K. Nosaki, K. Tomioka, S. Hara, K. Hiruma, J. Motohisa and T. Fukui, *Appl. Phys. Express*, 2009, **2**, 035004.
25 M. C. Putnam, M. A. Filler, B. M. Kayes, M. D. Kelzenberg, Y. B. Guan, N. S. Lewis, J. M. Eiler and H. A. Atwater, *Nano Lett.*, 2008, **8**, 3109–3113.
26 B. Balakrisnan, S. Patil and E. Smela, *J. Micromech. Microeng.*, 2009, **19**, 047002.